



16 **Abstract**

17 Understanding the behaviour of highly radiotoxic, long half-life radionuclide neptunium in  
18 the environment is important for the management of radioactively contaminated land and the  
19 safe disposal of radioactive wastes. Recent studies have identified that microbial reduction  
20 can reduce the mobility of neptunium *via* reduction of soluble Np(V) to the poorly soluble  
21 Np(IV), with coupling to both Mn(IV)- and Fe(III)- reduction implicated in neptunyl  
22 reduction. To further explore these processes Mn(IV) as  $\delta\text{MnO}_2$  was added to sediment  
23 microcosms to create a sediment microcosm experiment “poised” under Mn(IV)-reducing  
24 conditions. Enhanced removal of Np(V) from solution occurred during Mn(IV)-reduction,  
25 and parallel X-ray absorption spectroscopy (XAS) studies confirmed Np(V) reduction to  
26 Np(IV) during Mn(IV)-reduction. Molecular ecology analysis of the XAS systems, which  
27 contained up to 0.2 mM Np showed no significant impact of elevated Np concentrations on  
28 the microbial population. These results demonstrate the importance of Mn cycling on Np  
29 biogeochemistry, and clearly highlight new pathways to reductive immobilisation for this  
30 highly radiotoxic element.

31

## 32 **Introduction**

33 Internationally, deep geological disposal is being considered as the long-term management  
34 and disposal option for higher activity radioactive wastes (HAW). A fundamental knowledge  
35 of reactions between radionuclides and geomeia is essential to underpin the safety case for  
36 geodisposal. Neptunium is a key risk-driving radionuclide in HAW due to its long half life  
37 ( $^{237}\text{Np}$   $t_{1/2} = 2.1 \times 10^6$  years), ingrowth from  $^{241}\text{Am}$ , high radiotoxicity, and relatively high  
38 solubility as  $\text{Np(V)}$ . Indeed,  $\text{Np}$  is potentially the most mobile transuranic species in  
39 environments pertinent to deep geological disposal (e.g. Choppin and Stout, 1989; Kaszuba  
40 and Runde, 1999; Lloyd et al., 2000; Choppin, 2007; Law et al., 2010); further,  $\text{Np}$  is a  
41 persistent contaminant at or near nuclear sites (e.g., Cantrell, 2009; Morris et al., 2000;  
42 Stamper et al., 2013).

43 Neptunium is redox active and its environmental mobility can be affected by the  
44 biogeochemistry and redox conditions in the subsurface (Kaszuba and Runde, 1999; Lloyd et  
45 al., 2002; Choppin, 2007; Law et al., 2010). Under oxidising conditions  $\text{Np}$  is stable in  
46 solution as the soluble neptunyl cation,  $\text{NpO}_2^+$ , whilst under anaerobic conditions  $\text{Np}$  can be  
47 reduced to poorly soluble  $\text{Np(IV)}$  species (Kaszuba and Runde, 1999; Moyes et al., 2002;  
48 Llorens et al., 2005; Law et al., 2010; Bach et al., 2014). In the subsurface, microbial  
49 respiration can induce anaerobic conditions under which metals and radionuclides can be  
50 reduced (Lloyd and Renshaw, 2005). The development of bioreducing conditions is  
51 increasingly recognised as likely to be significant in the deep subsurface around a geological  
52 disposal facility (Pedersen, 2000; Fredrickson and Balkwill, 2006; Rizoulis et al., 2012;  
53 Williamson et al., 2013; Behrends et al., 2012), and is the basis for remediation of  
54 contaminated land where problematic radionuclides (e.g.  $\text{Tc}$  and  $\text{U}$ ) may be reduced either  
55 enzymatically or indirectly *via* interactions with reduced species (e.g.  $\text{Fe(II)}$ ): Lloyd et al.,  
56 2002; Lloyd, 2003; Gadd, 2010; Newsome et al., 2014).

57 The ability of microorganisms to enzymatically reduce Np(V) to Np(IV) has been  
58 demonstrated in pure culture experiments (Lloyd et al., 2000; Icopini et al., 2007) although  
59 some microorganisms are unable to facilitate enzymatic Np(V) reduction (Songkasiri et al.,  
60 2002; Renshaw et al., 2005). Toxicity effects on selected metal-reducing bacteria are also of  
61 interest as studies with indigenous microorganisms highlight the tolerance of microorganisms  
62 to mM concentrations of Np (Law et al., 2010; Ams et al., 2013), whilst in pure culture  
63 experiments no toxicity effects were observed at Np concentrations less than 2mM (Ruggiero  
64 et al., 2005). In sediment systems, reductive immobilisation of Np(V) to Np(IV) has been  
65 observed during development of sediment anoxia with microbial metal reduction implicated  
66 in the reaction and with indirect (abiotic) reduction by Fe(II) shown to be possible (Law et al  
67 2010).

68 Manganese is ubiquitous in soils and rock forming minerals and therefore, although Np  
69 interactions with Mn(IV) minerals have been studied previously (Wilk et al., 2005), a deeper  
70 understanding of Np(V) behaviour during early metal reduction (Mn(IV)- and Fe(III)-  
71 reduction) is essential in understanding its environmental behaviour in both deep and shallow  
72 subsurface environments. In addition, the potential importance of Mn in environmental  
73 actinide chemistry is increasingly recognised with Mn linked to both Pu and U cycling  
74 (Powell et al., 2006; Hu et al., 2010; Wang et al., 2013; Wang et al., 2014). Here we examine  
75 the behaviour of Np in sediment systems amended with labile Mn(IV) ( $\delta\text{MnO}_2$ ) to allow  
76 microcosms to develop a period of extended or “poised” Mn reduction (Lovley and Philips,  
77 1988). As well conducting experiments at low Np concentrations, we also collected XAS  
78 data from parallel experiments run at higher concentrations of Np. This allowed assessment  
79 of Np speciation and local-coordination under defined biogeochemical conditions. Finally,  
80 16S rRNA gene analysis was performed to assess the response of the indigenous microbial  
81 communities to elevated Np concentrations.

82

## 83 **Experimental Section**

### 84 *Safety*

85 Neptunium ( $^{237}\text{Np}$ ) is a high radiotoxicity alpha-emitting radionuclide with beta/gamma  
86 emitting progeny. Work can only be conducted by trained personnel in a certified, properly  
87 equipped radiochemistry laboratory, following appropriate risk assessment. The possession  
88 and use of radioactive materials is subject to statutory control.

89

### 90 *Sample Collection*

91 Sediments were collected from an area located ~ 2 km from the Sellafield reprocessing site in  
92 Calder River Valley, Cumbria during September 2012 (Lat 54°26'30 N, Long 03°28'09 W).  
93 Sediments were representative of the Quaternary unconsolidated alluvial flood-plain deposits  
94 that underlie the Sellafield site (Law et al., 2010) and were collected in sterile containers,  
95 sealed, and stored at 4 °C prior to use (< 1 month).

96

### 97 *Bioreduction Microcosms with Low $\text{NpO}_2^+$ concentrations*

98 Sediment microcosms ( $10 \pm 0.1$  g Sellafield sediment,  $100 \pm 1$  ml groundwater; in triplicate)  
99 were prepared using a synthetic groundwater representative of the Sellafield region (Wilkins  
100 et al., 2007) but with added nitrate and manganese (2 mM  $\text{NaNO}_3$ , 2 mM  $\delta\text{MnO}_2$ ) and with  
101 0.17 mmols of bioavailable Fe(III) in the sediment. Sodium acetate was also added in  
102 stoichiometric excess (10 mM) as an electron donor, the groundwater was sterilised  
103 (autoclaved for 1 hour at 120 °C), purged with filtered 80 % / 20 %  $\text{N}_2$  /  $\text{CO}_2$ , and pH adjusted  
104 to pH 7 (*via* drop-wise addition of 0.5 M HCl or 1M NaOH). Sediments and sterile  
105 groundwater were then added to sterile 120 ml glass serum bottles (Wheaton Scientific, USA)  
106 and sealed with butyl rubber stoppers using aseptic technique. Neptunium, as  $^{237}\text{NpO}_2^+$

107 (20 Bq ml<sup>-1</sup>; 3.2 μM; oxidation state verified by UV-Vis analysis) was then spiked into each  
108 microcosm; thereafter, the microcosms were incubated anaerobically at 21 °C in the dark for  
109 38 days. Throughout the incubation, sediment slurry was periodically extracted using aseptic  
110 technique, under an O<sub>2</sub>-free, Ar atmosphere. The sediment slurry was centrifuged (15,000 g;  
111 10 minutes) to separate sediment and porewater samples and ~ 0.5 g of sediment was stored  
112 at - 80 °C for microbiological characterisation.

113

#### 114 ***Geochemical Analyses***

115 During microcosm sampling, total dissolved NO<sub>2</sub><sup>-</sup>, Mn, and Fe concentrations were measured  
116 with standard UV-vis spectroscopy methods on a Jenway 6715 spectrophotometer (Lovley  
117 and Philips, 1987; Goto et al., 1997; Viollier et al., 2000; Harris and Mortimer, 2002).  
118 Aqueous NO<sub>3</sub><sup>-</sup>, SO<sub>4</sub><sup>2-</sup>, ammonium and acetate were measured by ion chromatography  
119 (Dionex ICS5000). Total bioavailable Fe(III) and the proportion of extractable Fe(II) in the  
120 sediment was estimated by digestion of 0.1 g of sediment in 5 ml of 0.5 N HCl for 60 minutes  
121 followed by the ferrozine assay, with and without added hydroxylammonium chloride  
122 (Lovley and Phillips, 1987; Viollier et al., 2000). The pH and Eh were measured with an  
123 Orion 420A digital meter and calibrated electrodes. Standards were routinely used to check  
124 the reliability of all methods and typically, calibration regressions had R<sup>2</sup> ≥ 0.99. The  
125 elemental composition and bulk mineralogy of the sediment were determined by XRF  
126 (Thermo ARL 9400) and XRD (Philips PW 1050). Total organic carbon and total inorganic  
127 carbon were determined on a LECO CR-412 Carbon Analyser. The total <sup>237</sup>Np concentration  
128 in solution was measured by ICP- MS (Agilent 7500cx) using <sup>232</sup>Th as the internal standard.

129

#### 130 ***XAS Experiments***

131 Experiments were prepared to allow direct determination of Np speciation and local  
132 coordination environment in sediments under different geochemical conditions using X-ray  
133 Absorption Spectroscopy (XAS). Here, the elevated concentration of Np required for direct  
134 spectroscopic characterisation (0.2 mM Np(V) as  $\text{NpO}_2^+$  in 0.07 M HCl) was added to  
135 microcosms containing 1g of sediment and 10 ml of groundwater that were poised at oxic,  
136 nitrate-, Mn-, Fe(III)-, and sulfate-reducing conditions, respectively. After Np(V) addition,  
137 the microcosms were left to incubate for 1 week in the dark at 7 °C prior to geochemical  
138 sampling and subsequent freezing at – 80 °C. Two additional Mn-reducing systems were also  
139 established where sediments had been enhanced with the addition of 2 mM  $\delta\text{MnO}_2$ : (i) 0.2  
140 mM  $\text{NpO}_2^+$  was added to an oxic microcosm that was then left to progress to Mn-reducing  
141 conditions (verified by the presence of Mn in porewaters and the absence of detectable 0.5 N  
142 extractable Fe(II) in sediments) before freezing at -80 °C, and (ii) a parallel Mn-reducing  
143 microcosm (again with no detectable 0.5 N extractable Fe(II) in sediments) was sterilised by  
144 autoclaving (1 hour at 120 °C) prior to the addition of 0.2 mM  $\text{NpO}_2^+$ , which was frozen at -  
145 80 °C after 2 days of reaction. For XAS analysis, sediment samples were defrosted,  
146 centrifuged and ~ 0.5 g of sediment was packed (under anaerobic atmosphere if necessary)  
147 into airtight approved sample containers which were then triple contained and frozen until  
148 analysis. XAS analysis was conducted at the INE Beamline for Actinide Research at the  
149 ANKA synchrotron, Karlsruhe, Germany. Neptunium  $L_{\text{III}}$ -edge spectra (17610 eV) were  
150 collected in fluorescence mode by a 5 element solid-state Ge detector. Parallel K-edge  
151 measurements from a Zr foil were recorded for energy calibration. XANES data were  
152 collected for all samples and EXAFS data were collected for selected samples. Background  
153 subtraction, data normalisation and fitting to EXAFS spectra were performed using the  
154 software packages Athena and Artemis. The XANES edge-jump was tied to unity. Modeling  
155 of the EXAFS data in  $k^3$  range was completed between 3 and 9.5  $\text{\AA}^{-1}$ .

156

157 ***Microbial community analysis***

158 Samples from an oxic sediment, and a Mn-reducing sample were taken from both low Np  
159 (20 Bq ml<sup>-1</sup>; 3.2 μM) and high Np (1.3 kBq ml<sup>-1</sup>; 0.2 mM) microcosms and analysis  
160 performed using PCR-based 16S rRNA gene analysis.

161

162 ***Ribosomal Intergenic Spacer Analysis***

163 DNA was extracted from Np containing microcosm samples (200 μl) using a PowerSoil  
164 DNA Isolation Kit (MO BIO Laboratories INC, USA). The 16S-23S rRNA intergenic spacer  
165 region from the bacterial RNA operon was amplified as described previously using primers  
166 ITSF and ITSReub (Cardinale et al., 2004). The amplified products were separated by  
167 electrophoresis in Tris-acetate-EDTA gel. The DNA was stained with ethidium bromide and  
168 viewed under short-wave UV light. Positive microbial community changes identified by the  
169 RISA justified further investigation by DNA sequencing of 16S rRNA gene clone libraries.

170 ***Amplification of 16S rRNA gene sequences***

171 A fragment of the 16S rRNA gene (approximately 1490 b.p.) was amplified from samples  
172 using the broad-specificity primers 8F (Eden et al., 1991) and 1492R (Lane et al., 1985). PCR  
173 reactions were performed in thin-walled tubes using a BioRad iCycler (BioRad, UK). Takara  
174 Ex Taq Polymerase (Millipore, UK) was used to amplify DNA from the sample extract. The  
175 PCR amplification protocol used with the 8F and 1492R primers was: initial denaturation at  
176 94 °C for 4 minutes, melting at 94 °C for 30 seconds, annealing at 50 °C for 30 seconds,  
177 elongation at 72 °C for 3 minutes and 35 cycles, followed by a final extension step at 72 °C  
178 for 5 minutes. The purity of the amplified products was determined by electrophoresis in tris-



179 acetate-EDTA (TAE) gel. DNA was stained with ethidium bromide and viewed under short-  
180 wave UV light using a BioRad Geldoc 2000 system (BioRad, UK).

### 181 ***Cloning***

182 PCR products were purified using a QIAquick PCR purification kit (Qiagen, UK) and ligated  
183 directly into a cloning vector containing topoisomerase I-charged vector arms (Agilent  
184 Technologies, UK) prior to transformation into *E. coli* competent cells expressing Cre  
185 recombinase (Agilent Technologies, UK). White transformants that grew on LB agar  
186 containing ampicillin and X-Gal were screened for an insert using PCR. Primers were  
187 complementary to the flanking regions of the PCR insertion site of the cloning vector. The  
188 PCR method was: an initial denaturation at 94 °C for 4 minutes, melting at 94 °C for 30  
189 seconds, annealing at 55 °C for 30 seconds, extension at 72 °C for 1 minutes and 35 cycles,  
190 followed by a final extension step at 72 °C for 5 minutes. The resulting PCR products were  
191 purified using an ExoSap protocol, 2 µl of ExoSap mix (0.058 µl Exonuclease I, 0.5 µl  
192 Shrimp Alkaline Phosphatase and 1.442 µl H<sub>2</sub>O) was added to 5 µl of PCR product and  
193 incubated at 37 °C for 30 minutes followed by 80 °C for 15 minutes.

### 194 ***DNA sequencing and phylogenetic analysis***

195 Nucleotide sequences were determined by the dideoxynucleotide method. An ABI Prism  
196 BigDye Terminator Cycle Sequencing Kit was used in combination with an ABI Prism 877  
197 Integrated Thermal Cycler and ABI Prism 377 DNA Sequencer (Perkin Elmer Applied  
198 Biosystems, UK). Sequences (typically 900 base pairs in length) were analysed using  
199 Mallard (Ashelford et al., 2006) to check for presence of chimeras or sequencing anomalies.  
200 Operational taxonomic units (OTU) were determined at a 98 % sequence similarity level  
201 using Mothur (Schloss et al., 2009). The individual OTU sequences were analysed using the

202 sequencing database of known 16S rRNA gene sequences provided on the Ribosomal  
203 Database Project (Cole et al., 2009) to identify nearest neighbours.

204

## 205 **Results and discussion**

### 206 *Sediment characteristics*

207 The sediment was dominated by quartz, feldspars (albite and microcline), and sheet silicates  
208 (muscovite and chlorite). The sediment had a high Si content (36.3 wt %) and contained Al  
209 (6.77 %), Fe (3.71 %), K (2.67 %), Na (0.92 %), Mg (0.75 %), Ti (0.38 %), Ca (0.27 %), and  
210 Mn (0.09 %). The total organic carbon content of the sediment was 0.69 % and total carbon  
211 was 1.70 %. The concentration of 0.5 N HCl extractable Fe in the sediment was  
212  $17.1 \pm 1.6 \text{ mmol kg}^{-1}$  prior to incubation and the sediment pH was  $\sim 5$ .

213

### 214 *Neptunium behaviour during progressive bioreduction*

215 Manganese enriched (2 mM  $\delta\text{MnO}_2$ ) sediment microcosms amended with electron donor, and  
216 a Mn enriched sterile control microcosm, were spiked with 3.2  $\mu\text{M}$  Np(V) (20 Bq  $\text{ml}^{-1}$ ) and  
217 incubated over a 38 day period. Modelling of the initial groundwater chemistry in  
218 PHREEQC-2 (Specific Ionic Theory (SIT) database) predicted that the speciation of the Np  
219 in solution would be predominantly  $\text{NpO}_2^+$  (see supporting information S1). In the sterile-  
220 control system, the pH remained stable and bulk biogeochemical changes indicative of  
221 terminal electron acceptor progression were not observed (Figure 1 A-F). A release of Mn  
222 ( $\sim 0.2 \text{ mM}$ ) into the groundwater of the sterile control occurred when the sediments were  
223 autoclaved (Figure 1C) which is similar to past studies with this material (Thorpe et al.,  
224 2012). In the microbially-active Mn rich microcosms, terminal electron accepting processes  
225 progressed in the order  $\text{NO}_3^- > \text{NO}_2^- > \text{Mn(IV)} > \text{Fe(III)} > \text{SO}_4^{2-}$  reduction as expected  
226 (Figure 1B-E). In all microcosms, the pH remained circumneutral (Figure 1F),  $\text{NO}_3^-$

227 decreased to  $< 0.2$  mM within 11 days, and porewater Mn increased to between  $0.05 - 0.1$   
228 mM after 9 days suggesting concomitant  $\text{NO}_3^-$  and Mn reduction in these systems (Figure  
229 1C). Microbially-mediated Fe(III) reduction was then evident after 17 days as indicated by  
230  $0.5$  N HCl extractable Fe(II) ingrowth to sediments. Importantly, in this system Mn  
231 reduction (indicated by Mn(II) in porewaters) occurred independently of any measurable  
232 Fe(III) reduction (indicated by a lack of Fe(II) ingrowth to sediments) across three time-  
233 points (days 7 to 11; Figure 1). The addition of  $2$  mM  $\delta\text{MnO}_2$  to sediments resulted in an  
234 extended Mn-reducing 'period' which was distinguished from the Fe(III)-reduction in the  
235 microcosm so that Np-behaviour could be tracked throughout the stages of early metal  
236 reduction. In the sterile control the added Np(V) was partially sorbed to the sediment, with  
237  $22.0$  % removed from solution after 7 days (Figure 1A). Thereafter, the concentration of Np  
238 in solution remained stable. Neptunyl sorption has been observed in to a similar extent in  
239 earlier studies using comparable sediment systems (Law et al., 2010) and has been attributed  
240 to sorption to negatively charged mineral surfaces (e.g. Fe(III)- or Mn(IV) -bearing minerals;  
241 Combes et al., 1992; Nakata et al., 2002; Arai et al., 2007; Müller et al., 2015; Wilk et al.,  
242 2005). In microbially active microcosms prior to the onset of Mn ingrowth to porewaters ( $0 -$   
243  $7$  days),  $43.0 \pm 1.9$  % of the added Np was removed from the groundwater (Figure 1A). By  
244 day 11 where Mn(IV)-reducing conditions had developed,  $86.0 \pm 4.9$  % of the added Np had  
245 been removed from solution. By the end of the experiment, following Fe(III) and subsequent  
246  $\text{SO}_4^{2-}$  reduction at 38 days  $96.1 \pm 0.5$  % of the added Np was removed to sediment.  
247 Enhanced removal of Np in active systems, compared to the sterile control, as observed in the  
248 first 7 days and prior to the onset of Mn reduction, could be attributed to either reduced  
249 surface reactivity in autoclaved sediments and / or enhanced Np(V) sorption to the system  
250 with microbial cells present (Gorman-Lewis et al., 2005; Ams et al., 2013). Results then  
251 show a clear relationship between Np(V) removal from solution and Mn reduction and

252 confirms that Np(V) is significantly removed from groundwater under Mn(IV)-reducing  
253 conditions. It remains unclear in these low Np microcosm studies whether Np(V) removal is  
254 linked to microbial metabolism or the result of abiotic reaction with Mn(II/III) minerals  
255 produced during microbial Mn(IV) reduction. The formation of Np-carbonatohydroxo  
256 complexes has been shown to increase the solubility of Np(IV) (Kitamura and Kohara, 2002;  
257 Kim et al., 2010). However, in these systems under end point sulfate reducing conditions (pE  
258 -4), and taking into account the increase in inorganic carbon expected from acetate utilization  
259 (2 mM), solution modelling in PHREEQC-2 (SIT database) predicted that Np would be  
260 speciated as Np(OH)<sub>4</sub> (see supporting information S2).

261

### 262 *Neptunium L<sub>III</sub>-edge XAS Experiments*

263 To assess the speciation of Np in sediment microcosms under different biogeochemical  
264 conditions, select samples were run at the elevated concentrations required for XAS analysis:  
265 oxic, nitrate-, Mn-, Fe(III)-, sulfate-, progressive Mn- and sterilized Mn- reducing. The  
266 XANES of Np in the sterile, oxic control sediment and in the NO<sub>3</sub><sup>-</sup> reducing sediment both  
267 showed a Np(V)-like spectra displaying the characteristic multiple scattering resonance  
268 structure at the high energy flank of the white line resulting from scattering along the axial  
269 oxygen atoms of the linear neptunyl moiety (Figure 2; Moyes et al., 2002; Denecke et al.,  
270 2005). Removal of Np from solution in both the oxic and nitrate reducing systems at  
271 circumneutral pH is occurring and is likely due to Np(V) sorption to Fe or Mn mineral  
272 surfaces (e.g. Combes et al., 1992; Nakata et al., 2002; Wilk et al., 2005; Arai et al., 2007;  
273 Law et al., 2010; Müller et al., 2015). By contrast, the XANES spectra for the progressive  
274 Mn-reducing microcosm, and the poised Mn(IV)-, Fe(III)-, and SO<sub>4</sub><sup>2-</sup>- reducing systems  
275 showed Np(IV)-like features with a loss of the multiple scattering resonance structure due to  
276 the loss of the two neptunyl dioxygenyl oxygen backscatterers (Figure 2). Here, the enhanced

277 removal of Np from solution compared to the oxic or nitrate-reducing systems is attributed to  
278 reductive precipitation of Np(V) to Np(IV) (Law et al., 2010). In the absence of defined  
279 (matrix-matched) standards for these complex systems, linear combination fitting of the  
280 microbially-active Mn-reducing systems (both progressively reduced, and poised), using the  
281 oxic sediment and the sulfate-reducing sediment as end-members, indicated that Np(IV) was  
282 indeed the dominant oxidation state in both systems (>90 % Np(IV)) (Ravel et al., 2005). In  
283 contrast, the XANES spectra for the sterile Mn-reduced microcosm was Np(V) like (> 90 %  
284 Np(V)). Interestingly, the presence of significant Np(IV) (~90 %) in the microbially-active  
285 Mn(IV)-reducing systems and dominant Np(V) (~ 90 %) in the sterile Mn(IV)-reducing  
286 sediments suggests that microbial reduction of Np(V) to Np(IV) is significant in reductive  
287 immobilisation of Np(V). Any artefacts associated with mineral reactivity and reducing  
288 capacity of the sterile Mn(IV)-reducing sediment resulting from autoclaving cannot be ruled  
289 out here, but the significant change in Np(V) reduction between the microbially active and  
290 sterile sediments suggests enzymatic processes are likely to play a role in controlling Np(V)  
291 reductive immobilisation. These observations on sterile Mn(IV)-reducing sediments differ  
292 from those observed in a sterilised Fe(III)-reducing sediment reacted with Np(V), which  
293 facilitated Np(V) reduction (Law et al., 2010) and supports observations by Wilk et al. (2005)  
294 that observed reduction of Np(V) by Mn(II) bearing minerals (manganite and hausmannite)  
295 did not occur naturally but was instead caused by the high energy X-ray beam.

296 EXAFS data were also collected from the sterile oxic and microbially-active Mn-, and  $\text{SO}_4^{2-}$ -  
297 reducing samples. The  $k^3$ -weighted EXAFS spectra and their Fourier transform spectra are  
298 shown together with the corresponding best model fits (Figure 3; Table 1). The best fit to the  
299 sterilised oxic control sample was a Np(V)-like coordination environment with two axial  
300 oxygen backscatterers at 1.85 Å and four equatorial oxygen backscatterers at 2.51 Å (Table 1,  
301 Figure 3). The atomic distances for both axial and equatorial oxygen backscatterers are within

302 the range reported for Np(V) (1.82 – 1.88 Å; Combes et al., 1992; Moyes et al., 2002;  
303 Denecke et al., 2005; Arai et al., 2007; Herberling et al., 2007; Law et al., 2010). The  
304 statistical relevance of additional shells, containing Fe, Mn or Np, was assessed using an F-  
305 test (Ravel et al., 2005) and it was found that no significant improvement to the model fit  
306 could be achieved. The sulfate reducing sample was modelled using a Np(IV) like  
307 coordination environment with eight oxygen backscatterers at a distance of 2.33 Å (Table 1,  
308 Figure 3; Llorens et al., 2005; Law et al., 2010). In agreement with the linear combination  
309 fitting, the best fit for the microbially active Mn(IV)-reducing sample was a Np(IV) like  
310 coordination environment like the sulfate reducing system with eight oxygen backscatterers  
311 at a distance of 2.31 Å. As with the oxic sediment sample, the addition of a second shell of  
312 Fe, Np or Mn did not significantly improve the fit when using the F test as a measure of  
313 validity. Finally it is noteworthy that in the samples where significant Np(IV) was present  
314 and where EXAFS was possible (the Mn(IV)-reducing sediment and sulfate-reducing  
315 microbially active sediments (Figure 3)), there was no evidence for a Np – O – Np interaction  
316 of the type that would be expected for nano-particulate NpO<sub>2</sub>, which has recently been  
317 observed in environmentally relevant systems (Husar et al 2015). These observations are in  
318 agreement with past work in sediment systems (Law et al 2010) which do not show  
319 significant evidence for a Np – O – Np interaction.

320

### 321 ***Microbial community analysis***

322 Analysis of the microbial community in the Mn(IV)-reducing systems with low (3.2 µM) and  
323 high (0.2 mM) Np content was performed to provide insight into the toxicity of Np(V) in  
324 these systems. The biogeochemical trajectory was similar in sediments with both low and  
325 high concentrations of Np suggesting that Np(V) was not significantly toxic to the microbial  
326 community in these systems. These observations were supported by the RISA results, which

327 were similar across both low Np and high Np metal-reducing samples, and clone libraries for  
328 low and high Np samples, that confirmed broadly similar communities (Figure 4). Both high  
329 and low concentration Np experiments showed a decrease in biodiversity compared to the  
330 oxic sediment sample: clone libraries from the oxic sediment showed 34 operational  
331 taxonomic units (OTUs) from 71 clones whereas the biostimulated samples showed 7 OTUs  
332 from 92 clones in the low Np sample and 12 OTUs from 74 clones in the high Np sample.  
333 The clone libraries of both low and high Np concentration Mn-reducing samples were  
334 dominated (> 50 %) by members of the class *Bacillus*, including known denitrifying species  
335 consistent with the microcosms being primed with 2 mM nitrate prior to Mn reduction. The  
336 microorganisms responsible for Mn(IV) reduction could not be identified due to the  
337 complexity of the system.

338

### 339 **Conclusions**

340 Overall these data show that microbially-mediated Mn(IV)-reduction can lead to reductive  
341 immobilisation of Np(V) to Np(IV). The addition of bioavailable  $\delta\text{MnO}_2$  provides a useful  
342 approach for prolonging microbial Mn(IV) reduction and allowing discrimination between  
343 the impacts of microbially-mediated Mn(IV) and Fe(III) reduction on radionuclide  
344 biogeochemistry. Removal of Np during Mn reduction was further maintained during Fe(III)  
345 and sulfate reduction and near complete removal of Np from solution had occurred by the  
346 onset of sulfate reduction. XANES data confirmed reduction to Np(IV) when Np was  
347 exposed to microbially active Mn(IV), Fe(III) and sulfate reducing sediments.  
348 Thermodynamically, Mn(IV) reduction is a more favourable process than Fe(III) reduction  
349 and so is likely to occur prior to Fe(III) reduction in subsurface environments where electron  
350 donor is limited. Although not conclusive these results imply that Np reduction in these  
351 systems occurs in the presence of active Mn-reducing cells rather than abiotically through

352 reaction with Mn(II) bearing minerals. Reduction of Np(V) by metal-reducing bacteria may  
353 provide an additional mechanism for Np(V) removal from groundwater ahead of the  
354 development of robust Fe(III)-reducing conditions. Results show the importance of  
355 subsurface microbial manganese cycling on the speciation of neptunium. These data have  
356 relevance to the fundamental understanding of Np behaviour in the shallow and deep  
357 subsurface.

358

### 359 **Acknowledgments**

360 This work has been supported by the Natural Environmental Research Council grants  
361 NE/H007768/1 and NE/L000547/1, an EPSRC University of Manchester / Sellafield Ltd.  
362 KTA award for which we acknowledge Nick Atherton and the Sellafield Land Quality Team,  
363 and STFC award ST/K001787/1. We thank Paul Lythgoe and Alastair Bewsher at The  
364 University of Manchester, and Jörg Rothe (KIT-INE) for help with data  
365 acquisition. Beamtime was obtained from the ANKA Lightsource (proposal number ANS-  
366 85) with support from the EU Actinet Programme.

367

### 368 **References**

369 Ams, D.A., Swanson, J.S., Szymanowski, J.E.S., Fein, J.B., Richmann, M., Reed, D.T.  
370 (2013). The effect of high ionic strength on neptunium(V) adsorption to a halophilic  
371 bacterium. *Geochim. Cosmochim. Acta*, 110, 45-57.

372 Arai, Y., Moran, P. B., Honeyman, B.D., Davis, J.A. (2007). In situ spectroscopic evidence  
373 for neptunium(V)-carbonate inner-sphere and outer-sphere ternary surface complexes  
374 on hematite surfaces. *Environ. Sci. Technol.*, 41, 3940-3944.



- 375 Ashelford, K.E., Chuzhanova, N.A., Fry, J.C., Jones, A.J., Weightman, A.J. (2006). New  
376 screening software shows that most recent large 16S rRNA gene clone libraries  
377 contain chimeras. *Appl. Environ. Microbiol.*, 72, 5734–5741.
- 378 Bach, D., Christiansen, B.C., Schild, D., Geckeis, H. (2014). TEM study of green rust sodium  
379 sulfate (GRNa<sub>2</sub>SO<sub>4</sub>) interacted with neptunyl ions (NpO<sub>2</sub><sup>+</sup>). *Radiochim. Acta*, 102(4),  
380 279-290.
- 381 Behrends, T., Krawczyk-Bärsch, E., Arnold, T. (2012). Implementation of microbial processes  
382 in the performance assessment of spent nuclear fuel repositories. *Appl. Geochem.*, 27,  
383 453-462.
- 384 Cantrell, K.J. (2009). Transuranic contamination in sediment and groundwater at the U.S.  
385 DOE Hanford site. US Department of Energy Report: PNNL-18640. Available at:  
386 [http://www.pnl.gov/main/publications/external/technical\\_reports/PNNL-18640.pdf](http://www.pnl.gov/main/publications/external/technical_reports/PNNL-18640.pdf)
- 387 Cardinale, M., Brusetti, L., Quatrini, P., Borin, S., Puglia, A.M., Rizzi, A., Zanardini, E.,  
388 Sorlini, C., Corselli, C., Daffonchio, D. (2004). Comparison of different primer sets  
389 for use in automated ribosomal intergenic spacer analysis of complex bacterial  
390 communities. *Appl. Environ. Microbiol.*, 70, 6147–6156.
- 391 Choppin, G.R., Stout, B.E. (1989). Actinide behaviour in natural waters. *Sci. Tot. Environ.*,  
392 83, 203-216.
- 393 Choppin, G.R. (2007). Actinide speciation in the environment. *J. Radioanal. and Nucl.*  
394 *Chem.*, 273, 695–703.
- 395 Cole, J.R., Wang, Q., Cardenas, E., Fish, J., Chai, B., Farris, R.J., Kulam-Syed-Mohideen,  
396 A.S., McGarrell, D.M., Marsh, T., Garrity, G.M., Tiedje, J.M. (2009). The Ribosomal  
397 Database Project: improved alignments and new tools for rRNA analysis. *Nucleic*  
398 *Acids Res.*, 37, 141-145.

- 399 Combes, J.M., Chisholm-Brause, C.J., Brown, G.E., Parks, G.A., Conradson, S.D., Eller,  
400 P.G., Triay, I.R., Hobart, D.E., Miejer, A. (1992). EXAFS spectroscopic study of  
401 neptunium(V) sorption at the  $\alpha$ -iron hydroxide oxide  $\alpha$ -FeOOH/water interface.  
402 *Environ. Sci. Technol.*, 26(2), 376-382.
- 403 Denecke, M.A., Dardenne, K., Marquardt, C.M. (2005). Np(IV)/Np(V) valence  
404 determinations from Np L3-edge XANES/EXAFS. *Talanta*, 65, 1008–1014.
- 405 Eden, P.E., Schmidt, T.M., Blakemore, R.P., Pace, N.R. (1991). Phylogenetic analysis of  
406 *Aquaspirillum magnetotacticum* using polymerase chain reaction-amplified 16S  
407 rRNA-specific DNA. *Int. J. Syst. Bacteriol.*, 41, 324-325.
- 408 Fredrickson, J.K., Balkwill, D.L. (2006). Geomicrobial processes and biodiversity in the deep  
409 terrestrial subsurface. *Geomicro. J.*, 23, 345-356.
- 410 Gadd, G.M. (2010). Metals, minerals and microbes: geomicrobiology and bioremediation.  
411 SGM prize lecture. *Microbiol.*, 156, 609-643.
- 412 Gorman-Lewis, D., Fein, J.B., Soderholm, L., Jensen, M.P., Chiang, M.H. (2005).  
413 Experimental study of neptunyl adsorption onto *Bacillus subtilis*. *Geochim.*  
414 *Cosmochim. Acta*, 69, 4837-4844.
- 415 Goto, K., Taguchi, S., Fukue, Y., Ohta, K., Watanabe, H. (1997). Spectrophotometric  
416 determination of manganese with 1-(2-pyridylazo)-2-naphthol and a non-ionic  
417 surfactant. *Talanta*, 24, 752-753.
- 418 Harris, S.J., Mortimer, R.J.G. (2002). Determination of nitrate in small water samples by the  
419 cadmium-copper reduction method: A manual technique with application to the  
420 interstitial waters of marine sediments. *Int. J. Environ. Anal. Chem.*, 82, 369- 376.
- 421 Herberling, F., Denecke, M.A., Bosbach, D. (2008). Neptunium(V) co-precipitation with  
422 calcite. *Environ. Sci. Technol.* 42(2), 471-476.

- 423 Hu, Y., Schwaiger, L.K., Booth, C.H., Kukkadapu, R.K., Cristiano, E., Kaplan, D., Nitsche,  
424 H. (2010) Molecular interactions of plutonium(VI) with synthetic manganese-  
425 substituted goethite. *Radiochim. Acta*, 98, 655–663.
- 426 Husar, R., Hübner, R., Hennig, C., Martin, P.M., Chollet, M., Weiss, S., Stumpf, T., Zänker,  
427 H., Ikeda-Ohno, A. (2015) Intrinsic formation of nanocrystalline neptunium dioxide  
428 under neutral aqueous conditions relevant to deep geological repositories. *Chem.*  
429 *Commun.*, 51, 1301-1304.
- 430 Icopini, G.A., Boukhalfa, H., Neu, M.P. (2007). Biological reduction of Np(V) and Np(V)  
431 citrate by metal-reducing bacteria. *Environ. Sci. Technol.* 41(8), 2764-2769.
- 432 Kaszuba, J.P., Runde, W.H. (1999). The aqueous geochemistry of neptunium: Dynamic  
433 control of soluble concentrations with applications to nuclear waste disposal. *Environ.*  
434 *Sci. Technol.*, 33, 4427-4433.
- 435 Kim, B.Y., Oh, J.Y., Baik, M.H., Yun, J.I. (2010) Effect of carbonate on the solubility of  
436 neptunium in natural granitic groundwater. *Nuc. Eng. Technol.*, 42 (5), 552-561.
- 437 Kitamura, A., Kohara, Y., (2002) Solubility of neptunium(IV) in carbonate media. *J. Nuc. Sci.*  
438 *Technol.*, 3, 294-297.
- 439 Lane, D.J., Pace, B., Olsen, G.J., Stahl, D.A., Sogin, M.L., Pace, N.R. (1985). Rapid  
440 determination of 16S ribosomal-RNA sequences for phylogenetic analysis. *P. Nat.*  
441 *Acad. Sci. USA*, 82, 6955-6959.
- 442 Law, G. T. W., Geissler, A., Lloyd, J.R., Livens, F.R., Boothman, C., Begg, J.D.C., Denecke,  
443 M.A., Rothe, J., Dardenne, K., Burke, I.T., Charnock, J.M., Morris, K. (2010).  
444 Geomicrobiological redox cycling of the transuranic element neptunium. *Environ. Sci.*  
445 *Technol.*, 44, 8924-8929.

- 446 Llorens, I., Den Auwer, C., Moisy, P., Ansoborlo, E., Vidaud, C., Funke, H. (2005).  
447 Neptunium uptake by serum transferrin. *FEBS Journal*, 272, 1739-1744.
- 448 Lloyd, J.R., Yong, P., Macaskie, L.E. (2000). Biological reduction and removal of Np(V) by  
449 two microorganisms. *Environ. Sci. Technol.*, 34, 1297-1301.
- 450 Lloyd, J.R., Chesnes, J., Glasauer, S., Bunker, D.J., Livens, F.R., Lovley, D.R. (2002).  
451 Reduction of actinides and fission products by Fe(III)-reducing bacteria.  
452 *Geomicrobiol. J.*, 19, 103-120.
- 453 Lloyd, J.R. (2003). Microbial reduction of metals and radionuclides. *FEMS Microbiol. Rev.*,  
454 27, 411-425.
- 455 Lloyd, J.R., Renshaw, J.C. (2005). Bioremediation of radioactive waste: radionuclide-  
456 microbe interactions in laboratory and field-scale studies. *Curr. Opin. Biotechnol.*, 16,  
457 254-260.
- 458 Lovley, D. R., Phillips, E. J. P. (1988). Manganese inhibition of microbial iron reduction in  
459 anaerobic sediments. *Geomicrobiol. J.*, 6, 145-155.
- 460 Lovley, D.R., Phillips, E.J.P. (1987). Rapid assay for microbially reducible ferric iron in  
461 aquatic sediments. *Appl. Environ. Microbiol.*, 53, 1536-1540.
- 462 Morris, K., Butterworth, J.C., Livens, F.R. (2000). Evidence for the remobilization of  
463 Sellafield waste radionuclides in an intertidal salt marsh, West Cumbria, UK. *Estuar.*  
464 *Coast. Shelf S.*, 51, 613-625.
- 465 Moyes, L.N., Jones, M.J., Reed, W.A., Livens, F.R., Charnock, J.M., Mosselmans, J.F.W.,  
466 Hennig, C., Vaughan, D.J., Patrick, R.A.D. (2002). An X-ray absorption  
467 spectroscopy study of neptunium(V) reactions with mackinawite (FeS). *Environ. Sci.*  
468 *Technol.*, 36, 179-183.

- 469 Müller, K., Gröschel, A., Rossberg, A., Bok, F., Franzen, C., Brendler, V., Foerstendorf, H.  
470 (2015). In situ spectroscopic identification of neptunium(V) inner-sphere complexes  
471 on the hematite water interface. *Environ. Sci. Technol.*, 49, 2560-2567.
- 472 Nakata, K., Nagasaki, S., Tanaka, S., Sakamoto, Y., Tanaka, T., Ogawa, H. (2002). Sorption  
473 and reduction of neptunium(V) on the surface of iron oxides. *Radiochim. Acta*, 90(9-  
474 11), 665-669.
- 475 Newsome, L., Morris, K., Lloyd, J.R. (2014). The biogeochemistry and bioremediation of  
476 uranium and other priority radionuclides. *Chem. Geo.*, 363, 164-184.
- 477 Pedersen, K. (2000). Exploration of deep intraterrestrial microbial life: current perspectives.  
478 *FEMS Microbiol. Lett.*, 185, 9-16.
- 479 Powell, B.A., Duff, M.C., Kaplan, D.I., Field, R.A., Newville, M., Hunter, D.B., Bertsh, P.M.,  
480 Coates, J.T., Eng, P., Rivers, M.L., Serkiz, S.M., Sutton, S.R., Triay, I.R., Vaniman,  
481 D.T. (2006). Plutonium oxidation and subsequent reduction by Mn(IV) minerals in  
482 Yucca Mountain tuff. *Environ. Sci. Technol.*, 40(11), 3508-3514.
- 483 Ravel, B., Newville, M. (2005). ATHENA, ARTEMIS, HEPHAESTUS: Data analysis for X-  
484 Ray absorption spectroscopy using IFEFFIT. *J. Synchro. Rad.*, 12, 537-541.
- 485 Renshaw, J.C., Butchins, L.J.C., Livens, F.R., May, I., Charnock, J.M., Lloyd, J.R. (2005).  
486 Bioreduction of uranium: Environmental implications of a pentavalent intermediate.  
487 *Environ. Sci. Technol.*, 39, 5657-5660.
- 488 Rizoulis, A., Steele, H.M., Morris, K., Lloyd, J.R. (2012). The potential impact of microbial  
489 metabolism during the geodisposal of intermediate level waste. *Mineral. Mag.*, 76,  
490 3261-3270.

- 491 Ruggiero, C.E., Boukhalfa, H., Forsythe, J.H., Lack, J.G., Hersman, L.E., Neu, M.P. (2005).  
492 Actinide and metal toxicity to prospective bioremediation bacteria. *Environ.*  
493 *Microbiol.*, 7, 88-97.
- 494 Stamper, A., McKinlay, C., Coughlin, D., Laws, F. (2013). Groundwater Annual Report  
495 2012. Sellafield Ltd, Technical report: LQTD000032
- 496 Schloss, P.D., Westcott, S.L., Ryabin, T., Hall, J.R., Hartmann, M., Hollister, E.B.,  
497 Lesniewski, R.A., Oakley, B.B., Parks, D.H., Robinson, C.J., Sahl, J.W., Stres, B.,  
498 Thallinger, G.G., Van Horn, D.J., Weber, C.F. (2009). Introducing mothur: Open-  
499 source, platform-independent, community-supported software for describing and  
500 comparing microbial communities. *Appl. Environ. Microbiol.*, 75, 7537-7541.
- 501 Songkasiri, W., Reed, D.T., Rittmann, B.E. (2002). Bio-sorption of neptunium(V) by  
502 *Pseudomonas fluorescens*. *Radiochim. Acta*, 90, 785-789.
- 503 Thorpe, C.L., Law, G.T.W., Boothman, C., Lloyd, J.R., Burke, I.T., Morris, K. (2012).  
504 Synergistic effect of high nitrate concentrations on sediment bioreduction.  
505 *Geomicrobiol. J.*, 29, 484-493.
- 506 Viollier, E., Inglett, P.W., Hunter, K., Roychoudhury, A.N., Van Cappellen, P. (2000). The  
507 ferrozine method revisited: Fe(II)/Fe(III) determination in natural waters. *Appl.*  
508 *Geochem.*, 15, 785-790.
- 509 Wang, Z., Lee, S.W., Kapoor, P., Tebo, B.M. and Giammar, D.E. (2013). Uraninite oxidation  
510 and dissolution induced by manganese oxide: A redox reaction between two insoluble  
511 minerals. *Geochim. Cosmochim. Acta*, 100(1), 24-40.
- 512 Wang, Z., Xiong, W., Tebo, B.M. and Giammar, D.E. (2014). Oxidative UO<sub>2</sub> dissolution  
513 induced by soluble Mn(III). *Environ. Sci. Technol.*, 48 (1), 289-298.

- 514 Wilk, P.A., Shaughnessy, D.A., Wilson, R.E., Nitsche, H. (2005). Interfacial interactions  
515 between Np(V) and manganese oxide minerals manganite and hausmannite. *Environ.*  
516 *Sci. Technol.*, 39, 2608-2615.
- 517 Wilkins, M.J., Livens, F.R., Vaughan, D.J., Beadle, I., Lloyd, J.R. (2007). The influence of  
518 microbial redox cycling on radionuclide mobility in the subsurface at a low-level  
519 radioactive waste storage site. *Geobiol.*, 5, 293-301.
- 520 Williamson, A.J., Morris, K., Shaw, S., Byrne, J.M., Boothman, C., Lloyd, J.R. (2013).  
521 Microbial reduction of Fe(III) under alkaline conditions relevant to geological  
522 disposal. *Appl. Environ. Microbiol.*, 79(11), 3320-3326.
- 523

524 **Figure Legends**

525

526 **Figure 1.** Microcosm incubation time-series data (days 0-37). (A) Np in porewaters, (B)  
527  $\text{NO}_3^-$  in porewaters, (C) Mn in porewaters, (D) 0.5 N HCl % extractable sedimentary Fe as  
528 Fe(II), (E)  $\text{SO}_4^{2-}$  in porewaters. ■ = microbially active microcosms; ● = sterile control  
529 microcosms. Initial pH in all microcosms was ~ 7. Error bars represent  $1\sigma$  experimental  
530 uncertainty from triplicate microcosm experiments (where not visible error bars are within  
531 symbol size).

532

533 **Figure 2.** Np  $L_{III}$ -edge XANES spectra for Np amended sediments under different biological  
534 conditions. Spectra from oxic sediment, nitrate-reducing sediment and sterilised Mn-reducing  
535 sediment samples show the Np(V) like multiple scattering resonance structure resulting from  
536 high energy scattering along the axial oxygen atoms of the linear neptunyl moiety. Spectra  
537 from Mn-, Fe(III)-, sulfate- and progressive Mn-reducing sediment samples do not contain  
538 this feature and are therefore more typical of Np(IV) XANES.

539

540 **Figure 3.** EXAFS spectra and Fourier transforms (uncorrected for phase shift of  
541 backscattering atoms) for Np on sediments under different geochemical conditions. From top  
542 to bottom: oxic, Mn- and sulfate-reducing conditions. Black lines are  $k^3$ -weighted data and  
543 grey lines are the best model fits to the data.

544

545 **Figure 4.** Microbial community analysis of (A) Oxic sediment at 0 days; (B) Mn-reducing  
546 sediment amended with  $3.2 \mu\text{M } ^{237}\text{Np}$ ; (C) Mn reducing sediment amended with  $0.2 \text{ mM}$   
547  $^{237}\text{Np}$ .

548



549 **Table 1**  
 550 EXAFS modelling of Np L<sub>III</sub> edge spectra for Np associated with sediments under different  
 551 biogeochemical conditions.

	Path	Type	<i>CN</i>	<i>R</i> (Å)	$\sigma^2$ (Å <sup>2</sup> )	$X_v^2$	<i>R</i>
Oxic	1	O	2	1.86	0.006	59.8	0.0079
	2	O	4	2.45	0.021		
Mn Red	1	O	8	2.31	0.014	217.3	0.0130
Sul Red	1	O	8	2.34	0.012	98.9	0.0227

552 *CN* is the coordination number, *R* is the interatomic distance,  $\sigma^2$  is the Debye-Waller factor  
 553 (Å<sup>2</sup>),  $X_v^2$  reduced chi square value and *R* is the least squares residual and is a measure of the  
 554 overall goodness of fit.  
 555

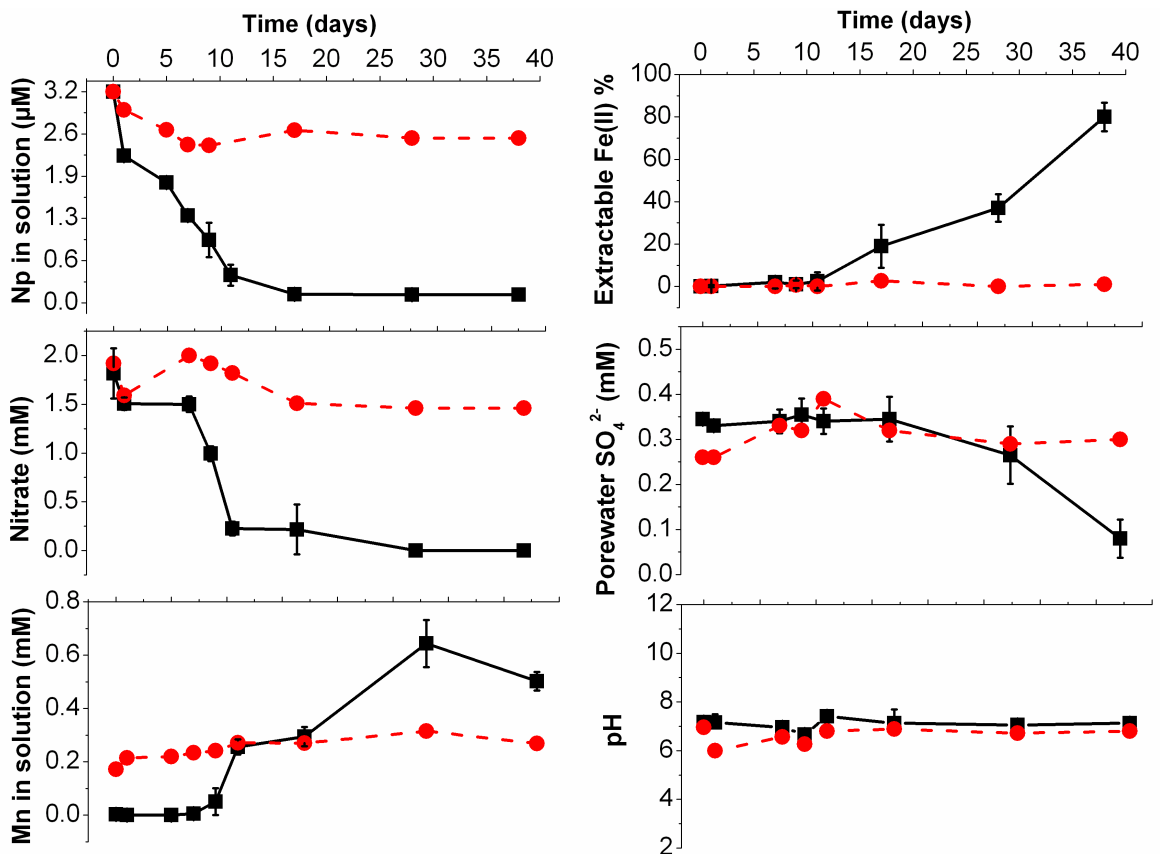
556

557

558

559

560 **Figure 1**



561

562

563

564

565

566

567

568

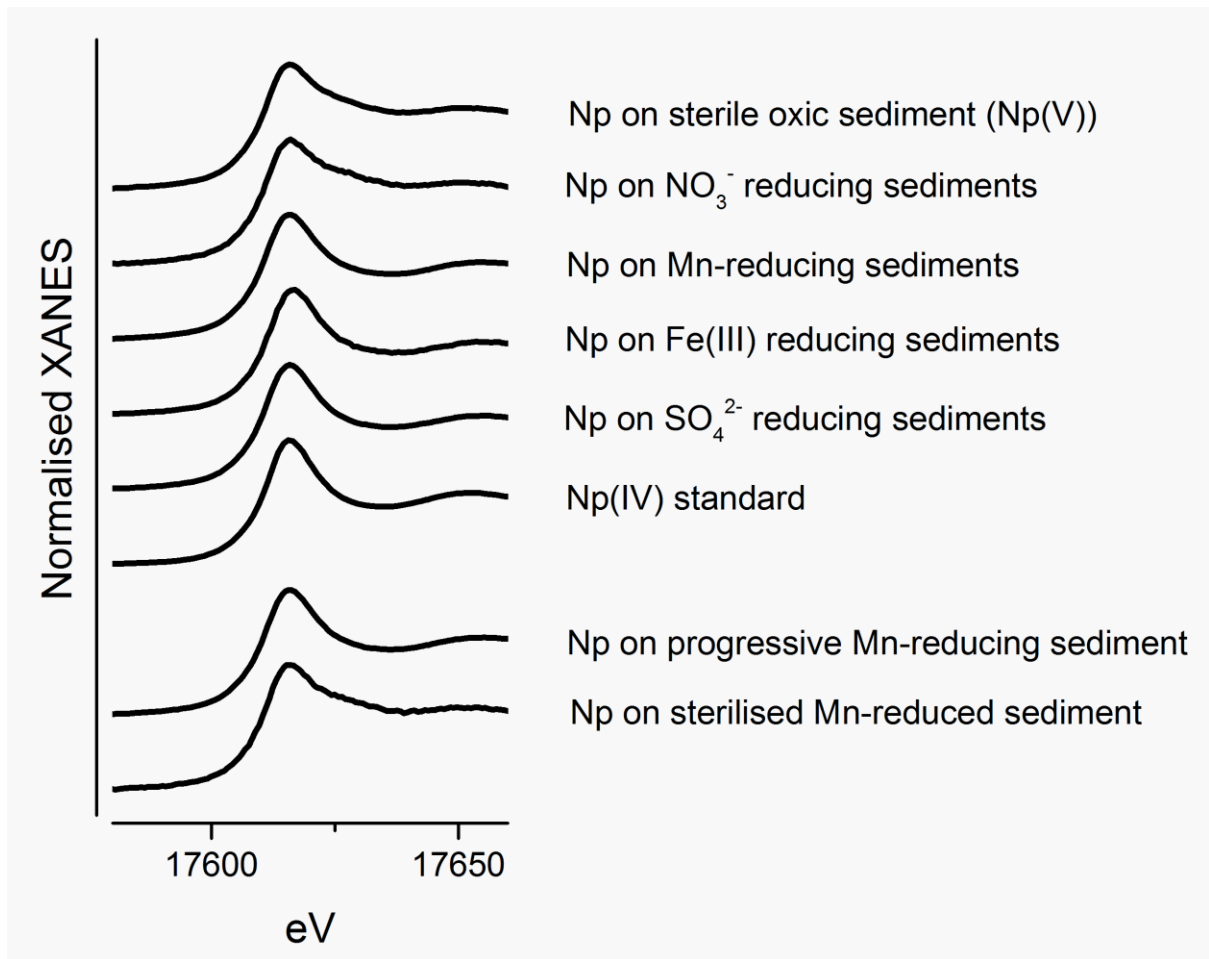
569

570

571

572

573



574

575 **Figure 2**

576

577

578

579

580

581

582

583

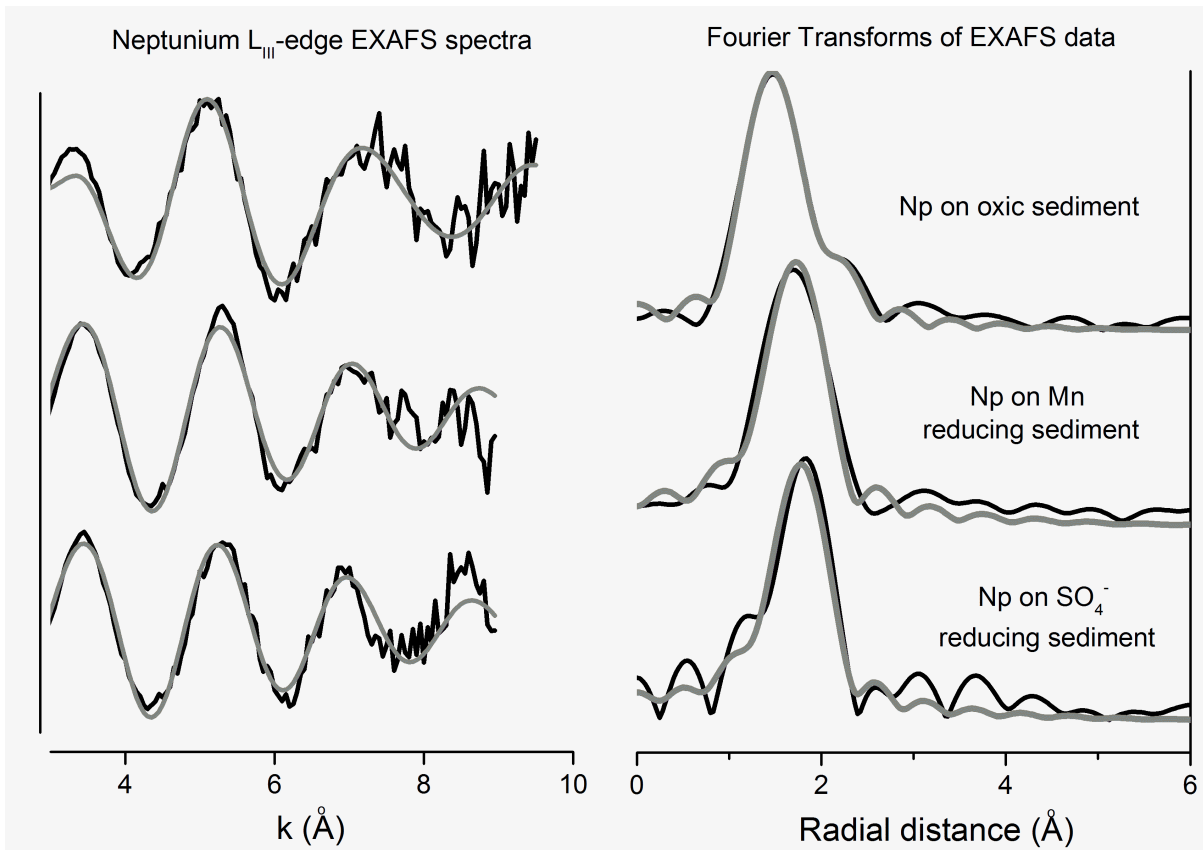
584

585

586

587

588



589

590

591 **Figure 3**

592

593

594

595

596

597

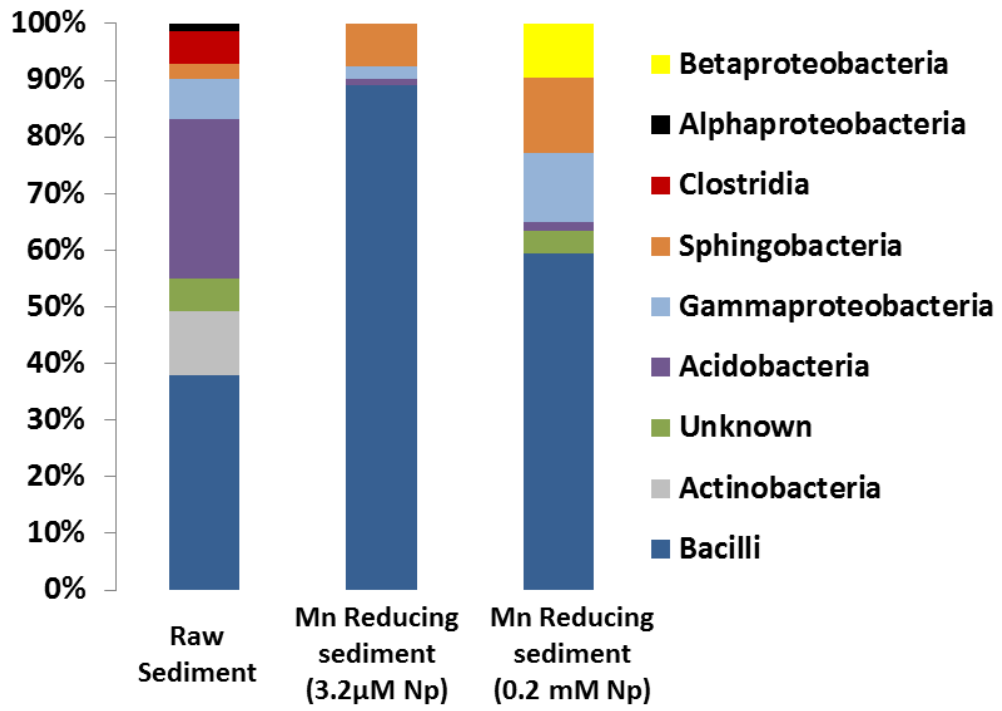
598

599

600

601

602

603 **Figure 4**

604

605

606